REPORT ON THE NATURAL OCCURRENCE OF A SILICA-CLAY NANOCOMPOSITE

István Dódony[1], Tibor Németh[1,2], Viktória K. Kis[3]

[1]Department of Mineralogy, Eötvös Loránd University, H-1117 Budapest, Pázmány Péter sétány 1/c
[2]Institute for Geological and Geochemical Research, Hungarian Academy of Sciences, H-1112 Budapest, Budaörsi út 45, Hungary
[3]Institute of Technical Physics and Materials Science, Centre for Energy Research, HAS, H-1121 Budapest, Konkoly Thege Miklós út 29–33, Hungary

A natural occurrence of a silica/clay nanocomposite material was investigated by transmission electron microscopy (TEM) and X-ray powder diffraction (XRD). High-resolution images show that this nanocomposite material consists of 5–20 nm thick slabs of smectite and tridymite/cristobalite layers with coincident normals. In spite of the brittle glass-like appearance of the nanocomposite material its colloidal properties are similar to those of pure smectite but partial loss of expansion capacity was detected upon glycerol solvation. The structural relationship between smectite and silica is interpreted based on the smectite structure model of Edelman and Favejee (1940) which supposes reversed tetrahedra in the SiO_4 layer of the TOT structure. This structure model explains the presence of silica impurities in bentonites used as raw material and several geological standard montmorillonites.

Keywords: silica, nontronite smectite, nanocomposite, transmission electron microscopy, structure model

Introduction

Smectites constitute a special group of layered silicates. They are nanocrystalline and have variable compositions leading to a net negative charge which is balanced by loosely bonded alkali or organic cations located on the interlamellar surfaces. These structural and chemical features are responsible for a set of unique properties including high cation exchange capacities, large chemically active surface area and unusual hydration characteristics, which form the basis for a wide range of applications. In addition, for a long time smectites have been used as precursor phases in the synthesis of polymer-clay nanocomposites [1].

Attempts to combine the properties of silica and clay result in highly porous clay heterostructures [2, 3]. By exchanging the interlayer Na^+ ions of montmorillonite with SiO_2-Fe_2O_3 mixed oxide sol particles extremely large surface areas and good thermal stability can be achieved [4]. The formation of silica nanorings suitable to be functionalized on the edges of clay particles has also been reported [5]. Another class of silica-clay nanocomposites with elemental silicate layers dispersed into a silica matrix are produced by the complete delamination of the clay precursor [6, 7].

Structure models of smectite are presented in *Figure 1*. Smectite is a three-layered clay mineral composed of two layers of silica tetrahedra (T) sandwiching a layer of (Fe, Mg, Al) octahedra (O) and these three layers form the structural unit called TOT. The normal of the TOT unit is parallel to the crystallographic **c** axis. According to the currently used smectite structural model [8], the vertices of the tetrahedra point towards the octahedral layer, resulting in an interlayer space between the basal planes of two neighbouring tetrahedral sheets. In the interlayer space there are hydrated exchangeable cations (*Figure 1a*).

As an alternative model, Edelman and Favejee [9] suggested that the tetrahedral orientation alternates in the T layers (*Figure 1b*), which means that every second tetrahedron is reversed with respect to the orientation proposed by the Hofmann et al. model, resulting in a tetrahedral arrangement similar to that in cristobalite and tridymite (*Figure 1c*). The reversed tetrahedra point towards the interlayer space and some apical oxygens are replaced by hydroxyl groups. Although the presence of Si-OH groups at the layer surfaces explains some properties of smectite including swelling or cation exchange, the Edelmann-Favejee model was mostly ignored by the mineralogy community.

Several decades later Eggleton [10] found reversed tetrahedra in stilpnomelane, an Fe-bearing layered silicate and explained this structural feature as a result of the misfit between the small SiO_4 tetrahedra and the large FeO_6 octahedra. Eggleton [11] later pointed out that if any smectite contains reversed tetrahedra as proposed by the Edelman-Favejee model, it would be the Fe-smectite with the mineral name nontronite.

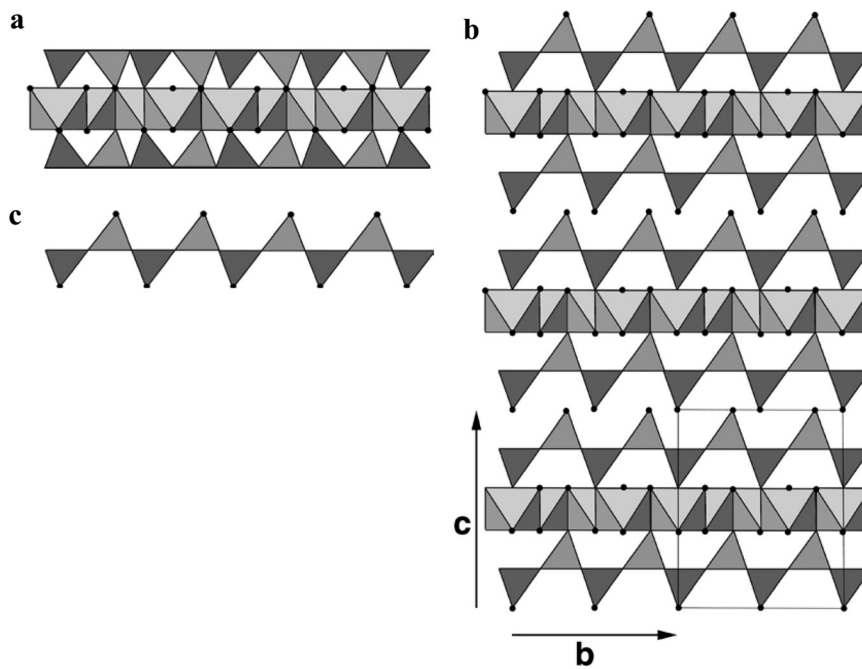* Corresponding author: Viktória K. Kis; E-mail: kis@mfa.kfki.hu

Fig. 1. Schematic structural models for smectite of (a) Hofmann et al. [8], (b) Edelman and Favejee [9], and the structural building unit of high-cristobalite and high-tridymite (c)

Dioctahedral smectites are frequently associated with cristobalite (e.g. [12, 13, 14, 15, 16]). In the XRD patterns of smectite/cristobalite associations cristobalite is represented by only one or two reflections (at 4.05 and 2.5 Å). Güven & Grim [13] made an attempt to separate the silica from smectite based on their different densities, but their subsequent XRD and TEM measurements proved that the two phases were inseparable in the majority of bentonites. Based on these observations a close structural relationship was supposed between smectite and cristobalite [17]. *hk*0 selected-area electron diffraction (SAED) patterns raised the possibility of an oriented intergrowth of the two phases [13, 15].

In this paper we report the natural occurrence of a novel type of a silica-clay nanocomposite material which contains ordered slabs of smectite and silica with similar dimensions. We present the results of high-resolution transmission electron microscopy (HRTEM) and X-ray diffraction studies and propose a structure model to explain the orientational relationship between silica and smectite.

Sample: origin, macroscopic and light microscopic features

A variety of the mineral chloropal from Hungary, historically called 'ungvárite' was investigated. The chloropal sample originates from the hydrothermally altered rhyolite tuff near Gönc, Tokaj-Eperjes Mountains, North East Hungary [18] and forms part of the mineral collection of the Natural History Museum at Eötvös University (inventory # K091039). The sample shows all macroscopic features of opals (conchoidal, sharp fracture, brittleness, hardness), has a light yellowish green colour, and
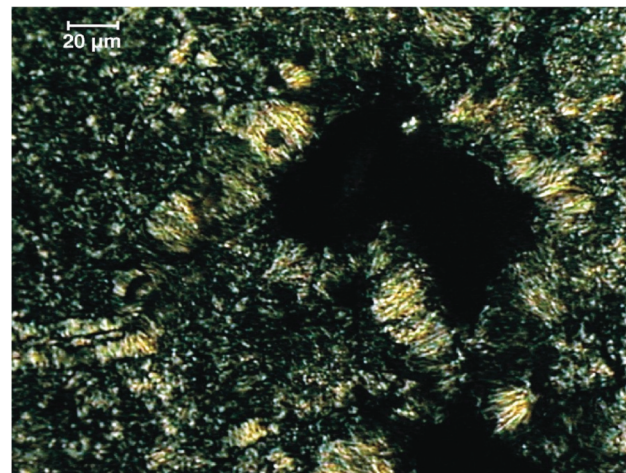

Fig. 2. Optical micrograph of the chloropal sample (crossed polars)

a slightly duller lustre than that of common opals. Under a petrographic microscope the sample shows equigranular texture with 1–2 μm grain size. At some places fibrous texture can be observed as well, the length of the fibres does not exceed 20 μm (*Figure 2*). The sample does not show any traces of weathering.

Experimental

X-ray diffraction measurements were carried out using a Philips PW 1710 diffractometer with Cu$_{K\alpha}$ radiation at 45 kV and 35 mA. Mineral composition of the bulk chloropal was determined on a random-powdered sample. Smectite was further characterized in details by XRD diagrams obtained from parallel-oriented specimens deposited onto

glass slides after various treatments. The following diagnostic treatments were carried out: ethylene glycol solvation at 60 °C overnight, Mg saturation followed by glycerol solvation at 95 °C overnight, K saturation, heating at 350 and 550 °C for 2 hours and Na saturation. The Green-Kelly (1953) test (Li saturation) was used to determine whether the layer charge originates from octahedral or from tetrahedral substitution. K saturation, subsequent heating to 110 °C and glycolization procedure was used to estimate the layer charge of the smectite. For K, Li, and Na 1 N, for Mg saturation 0.5 N chloride solution was used. Prior to X-ray diffraction analyses the prepared samples were stored under a controlled relative humidity (∼35% RH).

TEM studies were made using a JEOL 4000EX microscope operating at 400 keV. TEM specimens were mechanically thinned down to ca. 30 µm and finally ion beam milling was used to reach electron transparency.

Results and discussion

Based on the representative XRD pattern from the random powdered sample, chloropal is composed predominantly of smectite and tridymite, and minor amounts of cristobalite and quartz (*Figure 3a*).

The major components could be easily identified by their characteristic reflections in *Figure 3a*: basal reflection of smectite at around 15 Å, and reflections at 4.31, 4.11, 2.50 and 3.85 Å for tridymite reflections, the latter one being a shoulder on the high 2θ side of the 4.1 Å reflection. Similarly, quartz could be identified by its reflections at 3.34 and 1.82 Å. Quartz reflections are much sharper than the reflections of other phases,

indicating coherently scattering domain size differences between quartz and the other mineral components, quartz having a larger domain size. The intensity of 001 reflection of tridymite at 4.35 Å is higher than that of 100 reflection at 4.35 Å (indexed as high tridymite, according to Sato [19]. In the chloropal sample, however, the reflection around 4.1 Å is more intense than the other one at 4.3 Å. This can be explained with the presence of cristobalite, which 111 reflection contributes to the total intensity of the 4.1 Å peak.

The absence of the 003 smectite reflection around 5 Å suggests the presence of octahedral iron in the smectite structure, and the $d_{(060)}$ = 1.52 Å value coincides with those reported in the literature for nontronite [11, 20]. *Figure 3b* shows X-ray patterns from oriented samples followed by different solvation treatments. The sample swelled upon ethylene glycol solvation, and fully expanded to 17.2 Å. However, when the solvating agent is glycerol, the expansion is not uniform, since the basal reflection at 15 Å is split into two reflections at around 17 and 15 Å. The positions of silica reflections did not change on glycolation and glycerolation. The Mg-saturated sample exhibited a sharp basal reflection, and correspondingly, 002 at 8.50 Å together with a very weak 003 at around 5.60 Å appeared upon glycolation. These data reveal the absence of interstratification (*Figure 3b*).

XRD patterns of the different cationic forms are shown in *Figure 3c*. The 001 reflection of the untreated sample is slightly broadened towards high angles with a maximum at around 14.3 Å suggesting Mg, as the main interlayer cation, however, a heteroionic interlayer composition is possible. The XRD results on ion exchanged and saturated samples indicate the smectite character of the chloropal. The basal
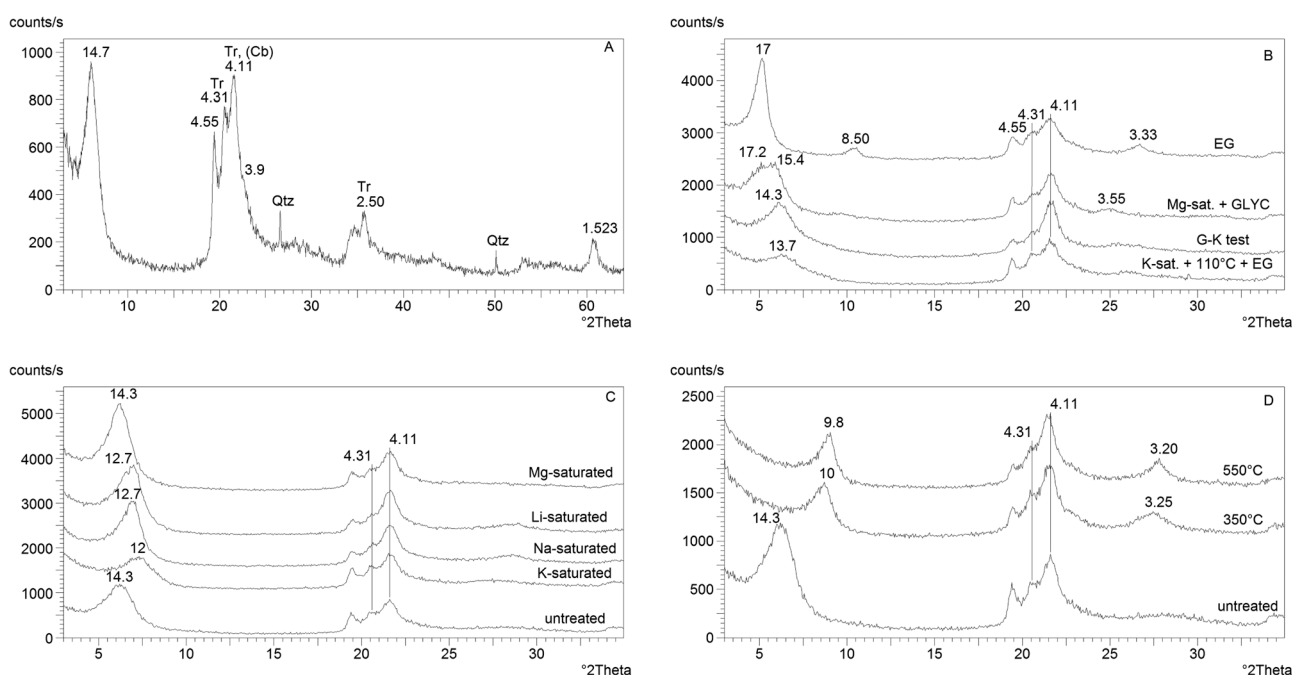

Fig. 3. X-ray diffraction patterns of cloropal samples subjected to various treatments: (a) a bulk disoriented sample in its original state, (b) samples after different solvations, (c) after cation saturations, and (d) after heat treatment. Tr = tridymite, Cb = cristobalite, Qtz = Quartz, EG = ethylene-glycol, GLYC = glycerol solvation, G-K test = Green-Kelly test

reflection shifted to 12 Å upon K saturation. Subsequent heating to 110 °C and glycolation caused partial expansion to around 14 Å, indicating medium layer charge. After the Green-Kelly test the sample re-expanded to 14.3 Å. Taking into account that the sample did not expand fully upon glycerol solvation even when it was Mg saturated, the result of this test indicates that the layer charge is allocated mainly to the tetrahedral sheets. Upon heating the sample to 350 °C and 550 °C, the smectite structure collapsed to 10 and 9.8 Å, respectively. The 100 tridymite reflection at 4.30 Å became slightly less distinct after heating to 550 °C (*Figure 3d*).

Electron diffraction patterns of chloropal were recorded in two orientations. If the electron beam is perpendicular to the TOT units of smectite, the SAED pattern is composed of diffraction rings with uneven intensity distribution. Such diffraction patterns are characteristic for smectites with turbostratic structure (e.g. [21]).

In the SAED pattern of chloropal (*Figure 4*) the most intense diffraction ring is at 4.5 Å, which corresponds to the 020 and 110 reflections of smectite. Further $hk0$ rings appear at 2.6 Å and 1.6 Å, corresponding to $d_{(200)}$ and $d_{(310)}/d_{(060)}$, respectively. The $d_{(100)}$ and $d_{(111)}$ of tridymite and cristobalite fall fairly close to the 020/110 smecite ring. In case of some disorder, which leads to broadening and thus blurring of the diffraction rings, close interplanar spacings of smectite and silica rings cannot be resolved. The ring at 3.5 Å is not continuous. According to the sparsely available X-ray diffraction data on dioctahedral smectites, nontronite $d_{(11-2)}$ falls between 3.5 and 3.62 Å [20]. Consequently, the arc-shaped reflections at 3.5 Å in chloropal presumably belong to the smectite structure with a hkl or $0kl$ type index. (Note that the hkl indices with l being an integer different from zero arise from a unit cell with $c_0 = 10$ Å. In the high vacuum conditions of the microscope the interlayer water from
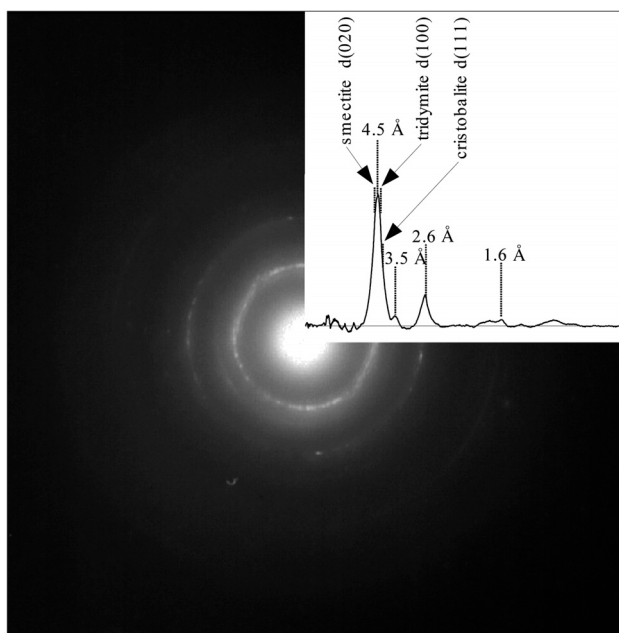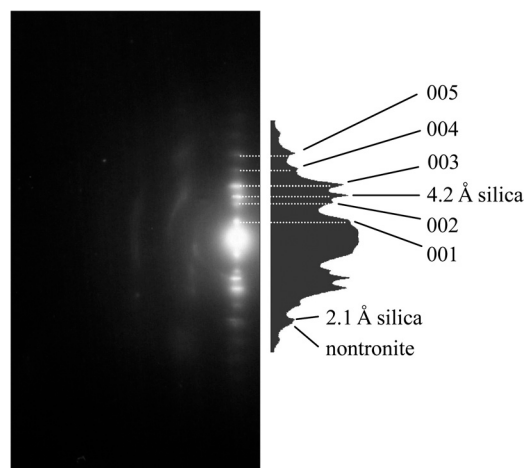

Fig. 5. SAED pattern of chloropal recorded parallel to the layer normal and a line profile measured along 00 l of nontronite. Nontronite indices refer to a dehydrated 10 Å structure. The pattern was taken from an area of about 250 nm of diameter. Note that separate reflections at 4.2 Å and 2.1 Å correspond to the thickness of a single tetrahedral sheet in tridymite/cristobalite

smectite escapes and a collapsed 10 Å periodicity along the **c** axis remains.)

Setting the electron beam parallel to the TOT units the (001) periodicity of dehydrated smectite is visible (10 Å) (*Figure 5*). Between the 002 and 003 reflections of the smectite the spacings of silica layers (4.2 Å) are clearly resolved. This spacing corresponds to the 002 and 111 reflections of the high temperature polymorph of tridymite and cristobalite, respectively (*Figure 1c*). Separate silica reflections appears at 2.1 Å as well. This diffraction pattern implies that chloropal is composed of smectite and silica layers with coincident normals.

The intimate intergrowth of silica with smectite is evident in high-resolution images shown in *Figure 6a*. 7–20 nm thick units of silica and smectite alternate in chloropal. However, the thickness of these packets is not uniform. There are parts where nontronite contains thinner silica units and vice versa. The periodicity in the silica units is close to 4.2 Å, the lattice fringes are roughly parallel to that of smectite. Smectite fringes are in places wavy, and terminate within the smectite unit (*Figure 6b*, shown by arrows).

The essential feature of the Edelman-Favejee model is the alternating orientation of tetrahedra in the six-membered rings in T sheets (*Figure 1b*). An 1/6 **b** shift between the neighbouring TOT units results in a cristobalite-like arrangement of tetrahedra in the "interlayer space". If the 1/6 **b** shift is combined with a 180° rotation in the (001) nontronite plane the result is a tridymite-like slab (*Figure 7a* and *b*). Such alternating tetrahedral orientations allow the formation of a nanocomposite material composed of nanometre-sized slabs of silica and clay. This nanocomposite preserves the cation exchange capacity and swelling of smectite, which is combined with the glass-like brittleness of silica.

Our results support Eggleton's idea [11] regarding the possible reversal of the tetrahedra in Fe-rich smectites, however, they do not rule out the validity of the Hofmann et al. [8] model. The main difference between the two models lies in
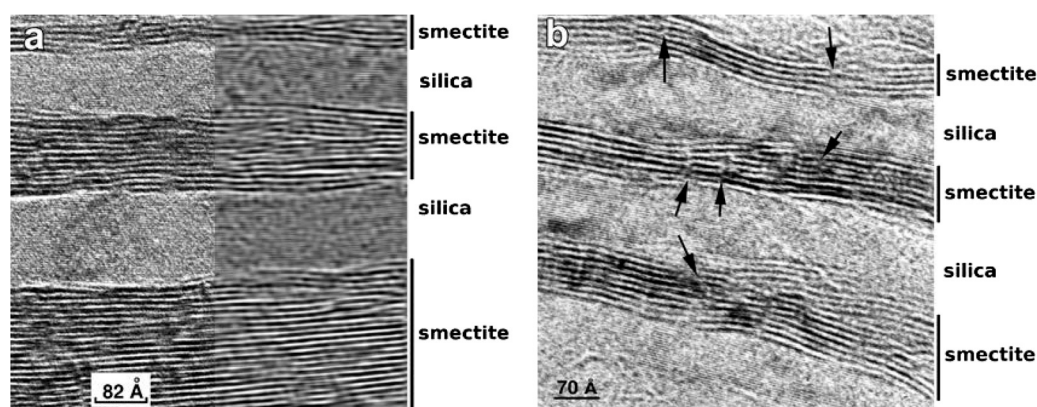

Fig. 4. Typical $hk0$ SAED pattern of chloropal. The inset shows radially integrated and background substracted intensity

Fig. 6. HRTEM images of chloropal showing the alternation of silica and smectite slabs. The left part of the figure in (a) shows an experimental image and the right part its lattice filtered inverse Fourier transform. Only the 00 *l* reflections were used for the reconstruction, no high spatial frequency cut-off was applied. In (b), terminations of smectitic layers are shown by arrows
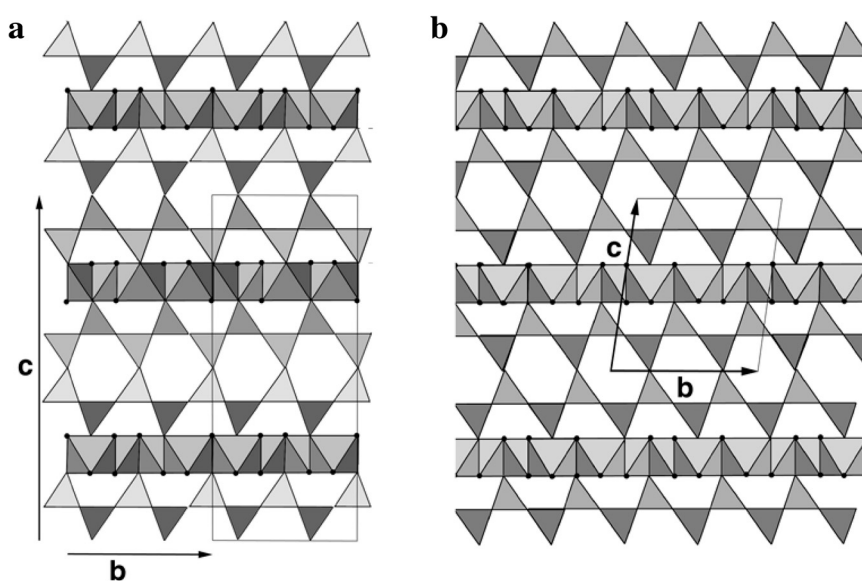

Fig. 7. Models for chloropal structures based on the Edelman-Favejee [9] structure model for smectite. An 1/6 *b* shift of the TOT unit combined with 180 degree rotation results in (a) tridymite-like, and without rotation in (b) cristobalite-like slabs

the sequence of atomic layers parallel to (001) smectite which manifests in the relative intensities of 00 *l* reflections. Measurement of 00 *l* intensities of well crystalline Fe-rich layer silicates would help the validation of the structure models.

the TOT unit of smectite and allows the interstratification of silica and iron smectite slabs that have an arbitrary thickness. The close structural relationship between silica and smectite explains why the two phases are inseparable in some clays.

Conclusions

Electron diffraction and high-resolution imaging of the mineral chloropal provide evidence for a novel type of silica-clay nanocomposite structure which has not been synthetized up to date. In this nanocomposite structure the 5–20 nm thick slabs of smectite and silica have coincident normals resulting in parallel (001) and (001)/(111) planes of Fe-smectite and tridymite/cristobalite, respectively. According to solvation experiments, the brittle, glass-like appearance of this nanocomposite material is associated with the colloidal properties of smectites.

Applying the early idea of Edelman and Favejee [9] we provide a structural model for this nanocomposite material. Our model proposes an alternating tetrahedral orientation in

Acknowledgements

References

1. Lambert J-F, Bergaya F: Smectite-polymer nanocomposites. In: Handbook of clay science, Eds: Bergaya F, Lagaly G, Elsevier (2006)
2. Galarneau A, Barodawalla A, Pinnavaia TJ: Porous clay heterostructures formed by gallery-templated synthesis. Nature 373, 529–531 (1995)

3. Polverejan M, Pauly TR, Pinnavaia TJ: Acidic porous clay heterostructures (pch): intragallery assembly of mesoporous silica in synthetic saponite clays. Chem Mater 12, 2698 (2000)

4. Han Y-S, Matsumoto H, Yamanaka, S: Preparation of new silica sol-based pillared clays with high surface area and high thermal stability. Chem Mater 9, 2013–2018 (1997)

5. Duan Q, Zhang J, Tian J, Zhao H: Silica nanorings on the surfaces of layered silicate. Langmuir 27, 13212–13219 (2011)

6. Letaief S, Ruiz-Hitzky E: Silica-clay nanocomposites. Chem Commun 24, 2996–2997 (2003)

7. Letaief S, Martín-Luengo MA, Aranda P, Ruiz-Hitzky E: A colloidal route for delamination of layered solids: novel porous-clay nanocomposites. Adv Funct Mat 16, 401–409 (2006)

8. Hofmann U, Endell K, Wilm D: Struktur und Quellung von Montmorillonit, das Tonmineral der Bentonittone. Z Kristallogr 86, 340–348 (1933)

9. Edelman CH, Favejee JChL: On the crystal structure of mont-morillonite and halloysite. Z Kristallogr 102, 417–431 (1940)

10. Eggleton RA: The crystal structure of stilpnomelane. Part II. The full cell. Miner Mag 38, 693–711 (1972)

11. Eggleton RA: Nontronite: chemistry and X-ray diffraction. Clay Minerals 12, 181–194 (1977)

12. Ross CS, Hendricks SB: Minerals of the montmorillonite group: Their origin and relation to soil clays. US Geol Surv Prof Pap 205-B, 23–79 (1945)

13. Güven N, Grim R: X-ray diffraction and electron optical studies on smectite and {alpha} -cristobalite associations. Clay Clay Miner 20, 89–92 (1972)

14. Viani A, Gualtieri AF, Artioli G: The nature of disorder in montmorillonite by simulation of X-ray powder patterns. Am Miner 87, 966–975 (2002)

15. Ilieva A, Dimov V: Montmorillonite-cristobalite association in bentonite clays from Bulgarian deposits. Proc of the Jubilee International Conference "80 years BGS", 71–74 (2005)

16. Lutterotti L, Voltolini M, Wenk H-R, Bandyopadhyay K, Vanorio T: Texture analysis of a turbostratically disordered Ca-montmorillonite. Am Miner 95, 98–103 (2010)

17. Nemecz E: Clay minerals. Akadémiai Kiadó, Budapest, 547 pp (1981)

18. Liffa A, Csajághy G: Subsequent occurrence of ungvárite (chloropal). Földtani Közlöny 77, 38–43 (1947) [in Hungarian]

19. Sato M: X-ray study of tridymite. Mineralogical Journal 4, 115–130 (1964)

20. Manceau A, Chateigener D, Gates WP: Polarized EXAFS, distance-valence least-squares modeling (DVLS), and quanti-tative texture analysis approaches to the structural refinement of Garfield nontronite. Phys Chem Minerals 25, 347–365 (1998)

21. Zvyagin BB: Electron diffraction analysis of clay mineral structures. Plenum Press, New York 364 pp (1967)